Clim Dyn (2008) 30:161–174
DOI 10.1007/s00382-007-0279-0

CO_2 threshold for millennial-scale oscillations in the climate system: implications for global warming scenarios

Katrin J. Meissner · Michael Eby · Andrew J. Weaver · Oleg A. Saenko

Received: 12 December 2006 / Accepted: 24 May 2007 / Published online: 15 June 2007

Abstract We present several equilibrium runs under varying atmospheric CO_2 concentrations using the University of Victoria Earth System Climate Model (UVic ESCM). The model shows two very different responses: for CO_2 concentrations of 400 ppm or lower, the system evolves into an equilibrium state. For CO_2 concentrations of 440 ppm or higher, the system starts oscillating between a state with vigorous deep water formation in the Southern Ocean and a state with no deep water formation in the Southern Ocean. The *flushing* events result in a rapid increase in atmospheric temperatures, degassing of CO_2 and therefore an increase in atmospheric CO_2 concentrations, and a reduction of sea ice cover in the Southern Ocean. They also cool the deep ocean worldwide. After the flush, the deep ocean warms slowly again and CO_2 is taken up by the ocean until the stratification becomes unstable again at high latitudes thousands of years later. The existence of a threshold in CO_2 concentration which places the UVic ESCM in either an oscillating or non-oscillating state makes our results intriguing. If the UVic ESCM captures a mechanism that is present and important in the real climate system, the consequences would comprise a rapid increase in atmospheric carbon dioxide concentrations of several tens of ppm, an increase in global surface temperature of the order of 1–2°C, local temperature changes of the order of 6°C and a profound change in ocean stratification, deep water temperature and sea ice cover.

Keywords Millenial-scale oscillations · Climate modelling · Nonlinear behavior of the climate system · Global warming scenarios · Carbon cycle

K. J. Meissner (✉) · M. Eby · A. J. Weaver
School of Earth and Ocean Sciences, University of Victoria, P.O. Box 3055, Stn CSC, Victoria, BC V8W 3P6, Canada
e-mail: katrin@ocean.seos.uvic.ca

O. A. Saenko
Canadian Centre for Climate Modelling and Analysis, Victoria, Canada

1 Introduction

Millennial-scale oscillations in the climate system, often referred to as Dansgaard-Oeschger cycles in the Northern Hemisphere and to A-events in the Southern Hemisphere, have been found in various paleoproxy records from the entire Northern Hemisphere, as well as in South America, New Zealand, Antarctica and the Southern Ocean (Hinnov et al. 2002; Leuschner and Sirocko 2000 and references therein). Although these oscillations are more pronounced under cold, glacial conditions, some records of the recent climate history indicate that millennial oscillations are also part of the Holocene climate. For example, ice-rafting events in the northern Atlantic recur at around 1,500-year intervals (Bond et al. 1997).

The cause of these abrupt changes in climate is still under investigation: whereas most climate scientists see changes in the strength of the North Atlantic thermohaline circulation (and subsequently changes in the oceanic meridional heat transport) as a plausible candidate (e.g. Clark et al. 2002), others state that variations in solar output might be the cause of the ''1,500-year'' cycles (Bond et al. 2001; Braun et al. 2005; also see Muscheler and Beer 2006 for a critical review of that theory). For example, Schmittner et al. (2003) combined reconstructions, climate model simulations and a conceptual model of the glacial climate change on millennial time scales to

examine the relationship between high latitude temperature changes of both hemispheres. Their conclusions emphasize the role of the thermohaline circulation in millennial-scale climate variability. Most of the available data and theories focus on the Northern Hemisphere, although there is increasing evidence for millennial timescale oscillations in the Southern Hemisphere (e.g. Partridge 2002; Kanfoush et al. 2000; Shackleton 2001; see also Sect. 4.2 in this paper).

In the 1980s and early 1990s, millennial-scale variability was analyzed in ocean models of varying complexity. Welander (1982) developed a vertical two-box model to study the oscillatory behavior caused by convective instability. Marotzke et al. (1988), and Marotzke (1989, 1990) analyzed millennial oscillations in a single-hemisphere ocean general circulation model under mixed boundary conditions. The system was switching between a state of weak meridional overturning (later called the ''decoupled'' mode where the deep ocean and the surface layers are decoupled) and a state of strong convection. During the decoupled state a polar halocline catastrophe (Bryan 1986) prevented the system from forming deep water. The deep ocean accumulated heat due to diffusion until eventually the water column became unstable and vigorous convection set in (''flushes'' or ''coupled mode'') and released the heat of the deep ocean that had accumulated over thousands of years. At the end of the flush, the system went into the decoupled mode again. Wright and Stocker (1991) demonstrated analytically that a steady diffusive state is unstable when using a linear equation of state in ocean models and therefore has to lead to a flush. A similar behavior was also found in other ocean models, which were all run under mixed boundary conditions (e.g. Weaver and Sarachik 1991; Winton 1993; Winton and Sarachik 1993; Winton 1995). Weaver and Hughes (1994) used an idealized global ocean model and added a stochastic component to the freshwater forcing. They showed that this random and short timescale forcing could trigger millennial-scale oscillations in the ocean model: the system was switching between three modes of North Atlantic Deep Water formation and stayed in each mode for up to a thousand years. At the same time, serious doubts concerning the use of mixed boundary conditions in ocean models and their role in density driven instabilities were raised (e.g. Zhang et al. 1993; Power and Kleeman 1994; Lenderink and Haarsma 1994). Modelling studies with coupled atmospheres of finite heat capacities (e.g. Mikolajewicz and Maier-Reimer 1994; Tziperman et al. 1994; Rahmstorf 1995) suggested that ''the ocean may have a lesser degree of internal thermohaline variability than portrayed in mixed boundary condition experiments when a fast restoring timescale is used on sea surface temperature'' (Weaver 1999). Winton (1997) and Sakai and Peltier (1997) showed that deep decoupling oscillations or flushes can exist under more realistic boundary conditions, in this case a 2D energy balance model combined with a fixed salt flux at the ocean's surface.

To the authors' knowledge, Haarsma et al. (2001) are the first modelling group which found millennial timescale oscillation in a model of intermediate complexity in which heat and fresh water fluxes are computed by a fully coupled atmosphere model. Although there are a multitude of studies with coupled atmosphere-ocean general circulation models (AOGCMs) which indicate that multiple steady states exist in the climate system, such a sustained millennial timescale oscillation has not been found in AOGCMs so far. An inherent problem with comprehensive AOGCMs is their computational expense. Simulations with AOGCMs are too expensive to be run long enough to reveal millennial timescale oscillations. As noted by Haarsma et al. (2001): ''the observed deep ocean temperature trends in AOGCMs are not necessarily a reflection of the fact that the AOGCM is not yet in equilibrium, but that they could be part of an ultra low-frequency oscillation.'' For a thorough historical review of millennial oscillations in ocean models, the reader is referred to Weaver and Hughes (1992), Weaver (1999) and Haarsma et al. (2001). Here, we present results of the UVic Earth System Model (UVic ESCM) which shows deep decoupled oscillations under certain climate conditions. As our model includes a fully coupled carbon cycle, we also quantify the effect of these oscillations on the carbon cycle and atmospheric CO_2. The model will be described in Sect. 2, the results will be analyzed in Sect. 3 and discussion and conclusions are given in Sects. 4 and 5, respectively.

2 Experimental setting

The UVic Earth System Climate Model (ESCM) consists of an ocean general circulation model (Modular Ocean Model, Version 2, Pacanowski 1995) coupled to a vertically integrated two dimensional energy-moisture balance model of the atmosphere, a dynamic-thermodynamic sea ice model based on Semtner (1976), Hibler (1979) and Hunke and Dukowitz (1997), a land surface scheme and a dynamic global vegetation model (Meissner et al. 2003). The model including the atmospheric, ocean and sea ice model is described in Weaver et al. (2001). It is driven by seasonal variations in solar insolation at the top of the atmosphere and seasonally-varying wind stress and wind fields (Kalnay et al. 1996). All experiments presented here are computed with near surface advection of specific humidity as described in Weaver et al. (2001). The wind field used for moisture advection is a humidity weighted average of long-term climatological monthly means from all of the NCEP

atmospheric levels available up to about 10,000 m (Kalnay et al. 1996). Radiative forcing associated with atmospheric CO_2 is applied in the model through a decrease in outgoing long wave radiation, parametrized as

$$F = F_0 \ln \frac{C(t)}{350}, \quad (1)$$

where $C(t)$ is the atmospheric CO_2 concentration at time t, and $F_0 = 5.35$ W/m^2 corresponds to a specified radiative forcing of 3.7 W/m^2 for a doubling of atmospheric CO_2 Ramaswamy et al. 2001]. The coupled model has a resolution of 3.6° in longitude and 1.8° in latitude and conserves both energy and water to machine precision without the use of flux adjustment.

The UVic ESCM also includes a fully coupled carbon cycle taking into account the terrestrial carbon fluxes and reservoirs (Meissner et al. 2003; Matthews et al. 2005) as well as the inorganic (Ewen et al. 2004) and organic (Schmittner 2005; Schmittner et al. 2005, 2007) carbon cycle in the ocean. The dynamic global vegetation model (DGVM) called 'TRIFFID' (Top-down Representation of Interactive Foliage and Flora Including Dynamics) was developed at the Hadley Centre for use in coupled climate-carbon cycle simulations (Cox et al. 2000) and is described in Cox (2001). TRIFFID defines the state of the terrestrial biosphere in terms of soil carbon, and the structure and coverage of five plant functional types (PFT): broadleaf tree, needleleaf tree, C_3 grass, C_4 grass and shrub. The areal coverage, leaf area index and canopy height of each PFT are calculated based on a 'carbon balance approach', in which vegetation change is driven by net carbon fluxes. These fluxes are derived for each vegetation type using the coupled photosynthesis-stomatal conductance model developed by Cox et al. (1999), which utilizes existing models of leaf-level photosynthesis in C_3 and C_4 plants (Collatz et al. 1991, 1992). TRIFFID is coupled to a land surface scheme which consists of a simplified version of 'MOSES' (Met Office Surface Exchange Scheme) and is described in (Meissner et al. 2003). The marine ecosystem/biogeochemical model is an improved NPDZ (nutrient, phytoplankton, zooplankton, detritus) model with a parameterization of fast nutrient recycling due to microbial activity (Schartau and Oschlies 2003). It includes two phytoplankton classes (nitrogen fixers and other phytoplankton), two nutrients (nitrate and phosphate), oxygen, dissolved inorganic carbon and alkalinity as prognostic tracers. A complete description of the ecosystem/biogeochemical model used for the present study can be found in Schmittner et al. (2007).

In this study, we use version 2.8 of the UVic ESCM to integrate 17 equilibrium simulations under varying atmospheric CO_2 concentrations ranging from 180 to 720 ppm. During these simulations, all forcing (continental ice sheets and orbital parameters) other than the radiative forcing due to atmospheric CO_2 was kept constant and equal to present day conditions. To include the effect of changes in wind and wind stress, anomalies were computed within the atmospheric model and added to the NCEP data (see Sect. 3.3 for an analysis of different wind forcings). As the model with the fully coupled carbon cycle is very expensive to run for long term simulations, we conducted the first 17 equilibrium simulations without the carbon cycle module. In Sect. 3.3 additional simulations are analyzed testing the parameter space of our simulations. Section 3.4 presents the results of a simulation comprising the carbon cycle.

3 Results

The 17 equilibrium simulations can be bundled into two different groups: for atmospheric CO_2 concentrations ranging from 180 to 400 ppm the model reaches a quasi-equilibrium state with no major oscillations. For atmospheric CO_2 concentrations of 440 ppm and higher, the model switches between two radically different quasi-stationary regimes: Long periods of weak overturning in the Southern Ocean associated with a slow warming of the deep ocean are interrupted by flushes of extremely strong deep water formation in the Southern Ocean. The frequency of the oscillations increases with increasing CO_2 forcing.

Figure 1a shows the time series of the globally averaged ocean potential temperature for each simulation with an atmospheric CO_2 concentration of 360 ppm or higher. For clarity, only one and a half cycles are shown for each experiment. Model results of the remaining 10 simulations (180–320 ppm) are similar to the 360 and 400 ppm experiments and are not shown. The model simulations have been run in each case for several thousand years before their results are shown in the time series and used for analysis. The global mean ocean potential temperature increases with increasing CO_2 concentrations in the atmosphere. Whereas most of the simulations reach a quasi equilibrium state, the five warmest runs show a strong oscillatory behavior on millennial timescales. Southern Hemisphere sea ice area is strongly reduced during the flushing events (Fig. 1b) and global averaged atmospheric surface temperatures show a warming of almost 1°C (Fig. 1c). The global mean density of kinetic energy is shown in Fig. 1d; it increases by 25% percent during the flushing events.

3.1 Southern Ocean flushes

The oscillatory behavior of the system is very similar for the five warmest simulations. We will focus our attention on only one of the simulations (atmospheric

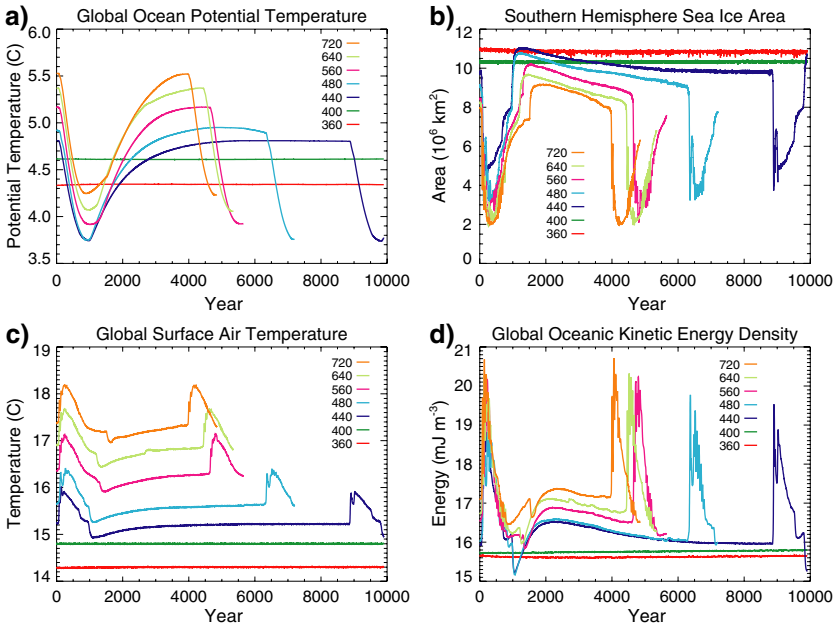

Fig. 1 Time series of the seven warmest equilibrium runs forced with different atmospheric CO_2 concentrations. **a** Global mean ocean potential temperature in °C, **b** southern hemispheric mean sea ice area in 10^6 km^2, **c** global mean atmospheric surface temperature in °C, **d** global mean density of kinetic energy in mJm^{-3}

CO_2 = 720 ppm) in this section for a further analysis of the dynamical behavior.

Figure 2 shows the mean potential temperature (Fig. 2a) and salinity (Fig. 2b) in the Southern Ocean south of 60°S during a flushing event (dashed line) and at a time step between two flushing events (solid line). Haline stratification is more pronounced in the decoupled state between flushes with a large freshwater anomaly at the surface. The temperature gradient reverses between the two states; while mid-depth and deep ocean potential temperatures are substantially warmer than surface temperatures in the decoupled state, potential temperature decreases with depth during the flushing event. The strength of the meridional overturning stream function is shown for both cases in Fig. 2c and d. Sea ice cover is reduced during the flush (compare Figs. 3a, b), and sea ice covers the deep water formation sites between flushes (Fig. 3c). Surface air temperature increases during the flushes, especially over regions where important changes in sea ice cover (and therefore surface albedo) occur (Fig. 3d).

Time series from one location in the Southern Ocean (1.8°E, 65.7°S) are shown in Fig. 4. Please note that the starting year of Figs. 1 and 4 differs. In Fig. 1 the time series for all experiments were aligned at the onset of a flush to facilitate the comparison between different simulations. Here we start the time series before the first shown flush, so that two full flushing events are well represented. Deep ocean potential temperatures increase between flushes and are cooled rapidly as soon as deep convection starts at that location (Fig. 4a, dashed line). We chose to show time series at 1.8°E, 65.7°S because this grid box lies within the region with the strongest convection events. However, this grid box is not one of the first ones to start convection at the beginning of each flushing event. Convection starts in surrounding regions several hundred years before the stratification at (1.8°E, 65.7°S) becomes unstable. Therefore, colder deep water is advected and diffused into the box analyzed in this study prior to the convection in the box, so that the deep ocean starts to cool gradually before convection starts.

Surface temperatures (Fig. 4a, solid line) are stable and at the freezing point between the flushing events. Due to convection (warm water from the deep ocean) and advection and diffusion (warm water from low latitudes) the surface temperatures increase during the flushes. Surface salinity (Fig. 4b, solid line) is low between flushes and increases mainly due to convection during the flushes. Sea ice cover (Fig. 4c) oscillates between 55% between flushes and 0% during convection events. The ventilation depth is shown in Fig. 4d, and surface heat and freshwater fluxes are shown in Fig. 4e and f. The heat loss of the ocean increases dramatically during the flushing events as there is no sea ice cover and the ocean surface temperatures are relatively high compared to atmospheric temperatures. The freshwater flux decreases during the flushes as evaporation increases with less sea ice cover.

Time series of potential temperature, salinity and density in the deep Southern Ocean south of 61.2°S (1,000 m depth to bottom) and at the surface south of 61.2°S (surface to 130 m) are shown in Fig. 5b and a, respectively. The temperature time series have been multiplied by $-\rho_0 \cdot \alpha$, salinity time series by $\rho_0 \cdot \beta$ to simplify the comparison between the salinity and potential temperature effect on potential density (the values chosen for α, β and ρ_0 are

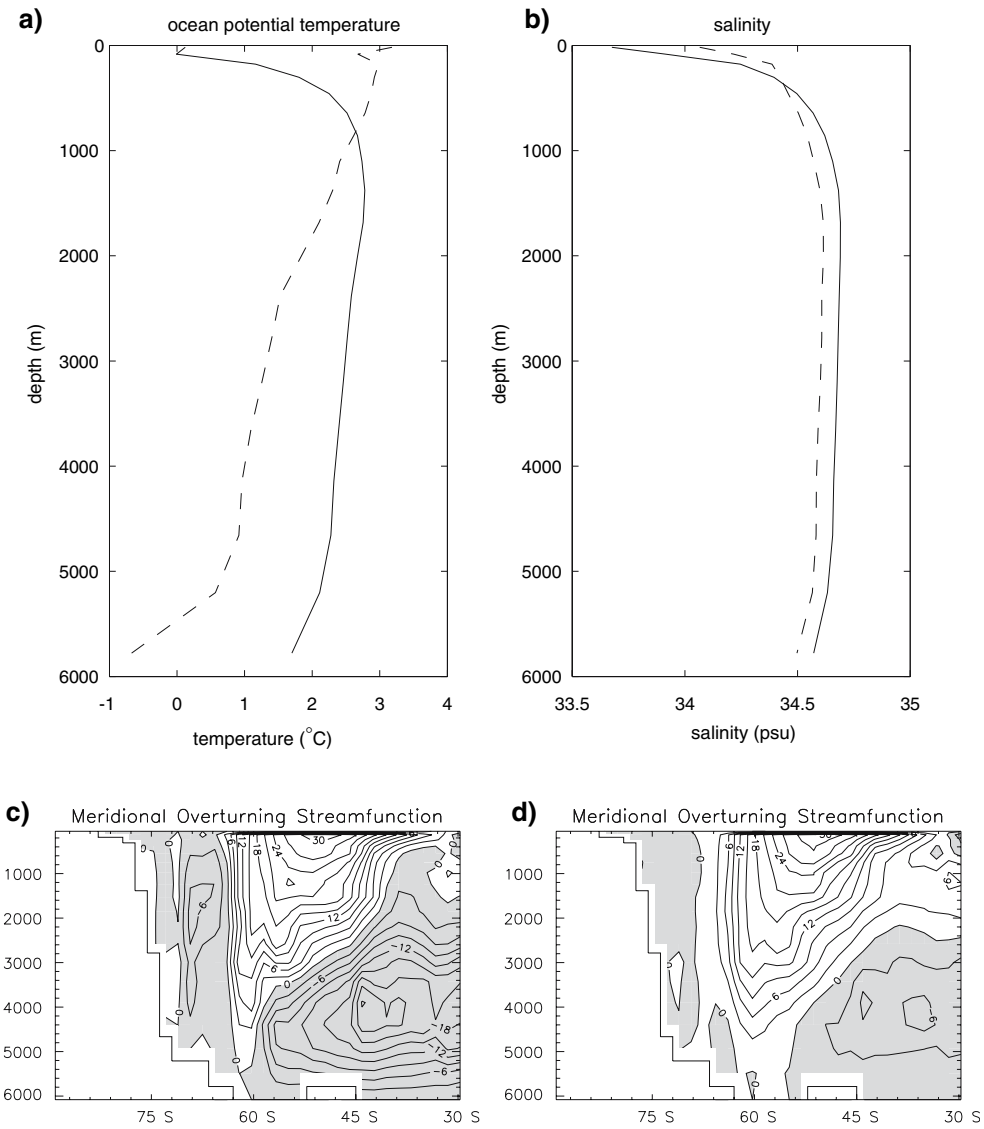

Fig. 2 Annual mean ocean potential temperature in °C south of 60°S (**a**) during a flushing event (coupled mode, *dashed line*) and between two flushing events (decoupled mode, *solid line*); annual mean ocean salinity in psu south of 60°S (**b**) during a flushing event (coupled mode, *dashed line*) and between two flushing events (decoupled mode, *solid line*); meridional overturning (in Sv) during a flushing event (**c**) and between two flushing events (**d**). Results from the equilibrium run with an atmospheric CO_2 concentration of 720 ppm

1.7×10^{-4}/K, 7.6×10^{-4} kg/g and 1,028 kg/m^3, respectively.). As can be seen in Fig. 5b, changes in potential density are mainly thermally driven in the deep ocean (factor 2 between thermal and haline driving). On the other hand, potential density changes are mainly salinity driven in the surface layers (Fig. 5a).

In conclusion, the system is showing oscillations on millennial timescales which have been described analytically by Wright and Stocker (1991) and are very similar to the oscillations described by Haarsma et al. (2001). Between two flushes, not only the deep Southern Ocean, but the entire deep ocean is warming due to diffusive processes. Sea ice and subsequently fresh surface waters (less evaporation due to sea ice cover) prevent deep convection in the Southern Ocean. The warming of the deep ocean in subpolar and polar regions eventually results in an unstable stratification, which than leads to extremely strong deep water formation and a thermally-driven circulation (Marotzke 1990; Weaver and Sarachik 1991). A schematic picture of the different processes involved in the dynamical behavior of the system is displayed as Fig. 8 in Haarsma et al. (2001) and reproduced here in Fig. 6.

3.2 Timescales

There are four major processes transporting heat vertically in the ocean model. These are due to large-scale circulation (LSC), mesoscale eddies (MSE), convection (CON) and small-scale turbulent mixing (SSM). Therefore, the rate of change of global mean potential temperature below a certain depth level can be written as

$$\frac{\partial <\theta>}{\partial t} = \mathrm{LSC} + \mathrm{MSE} + \mathrm{CON} + \mathrm{SSM} \qquad (2)$$

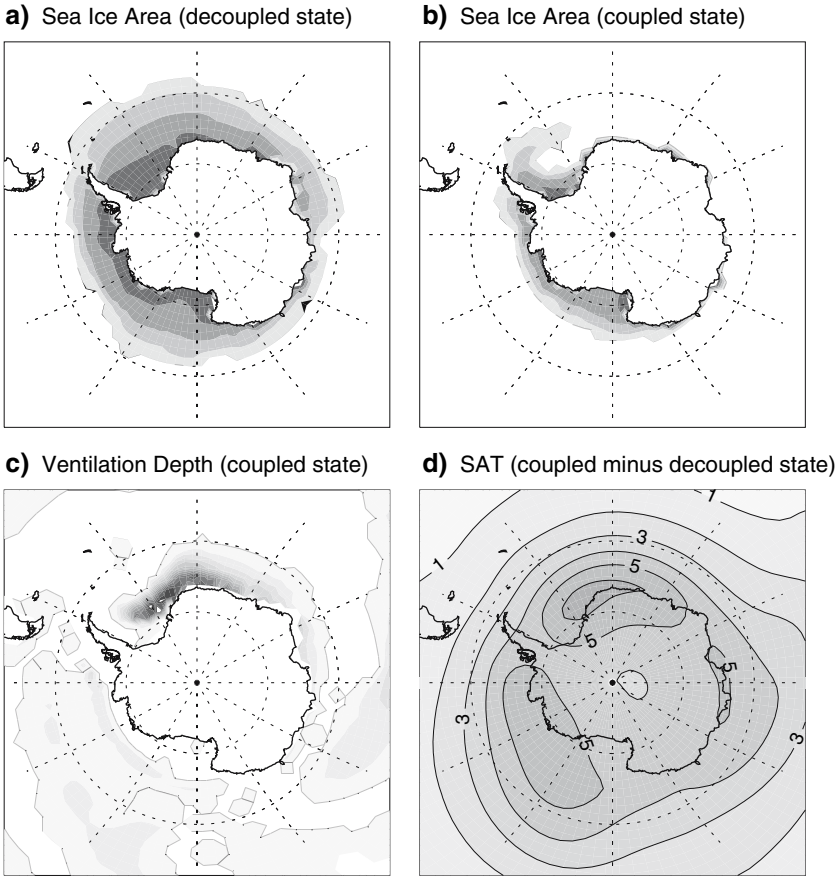

Fig. 3 Annual mean fields of area covered with sea ice between two flushing events (**a**) and during a flushing event (**b**); ventilation depth during a flushing event (**c**) and the difference of surface air temperature (coupled minus decoupled mode, in °C) (**d**). Results from the equilibrium run with an atmospheric CO_2 concentration of 720 ppm

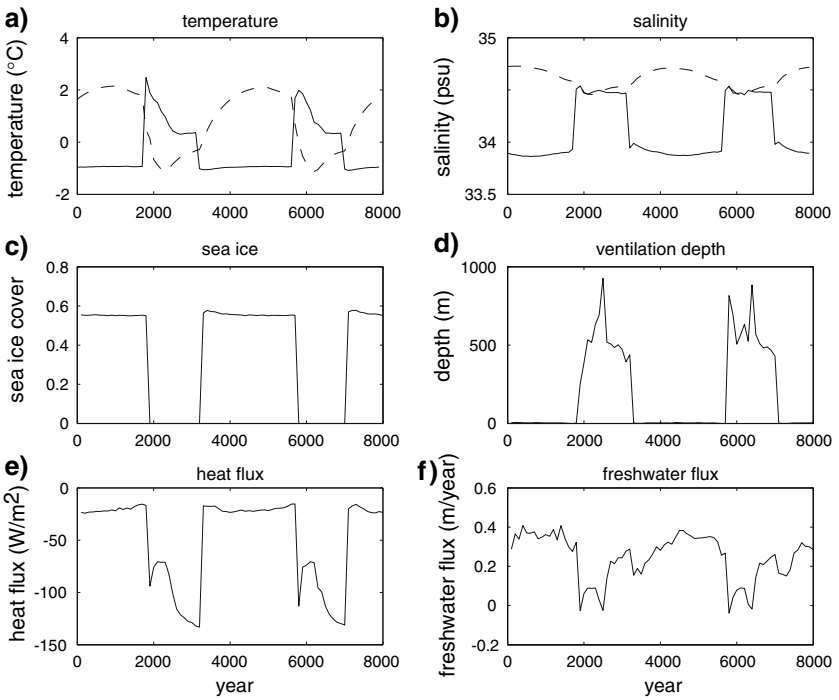

Fig. 4 Time series from the equilibrium run with an atmospheric CO_2 of 720 ppm in one location in the Southern Ocean (1.8°E, 65.7°S). **a** Potential ocean temperature (in °C) for the surface layer (17.5 m, *solid line*) and deep ocean (4,143 m, *dashed line*); **b** salinity (in psu) for the surface layer (17.5 m, *solid line*) and deep ocean (4,143 m, *dashed line*); **c** sea ice area fraction (1 = 100%); **d** ventilation depth (in m); **e** downward surface heat flux (in Wm^{-2}) and **f** downward surface freshwater flux (in m/year)

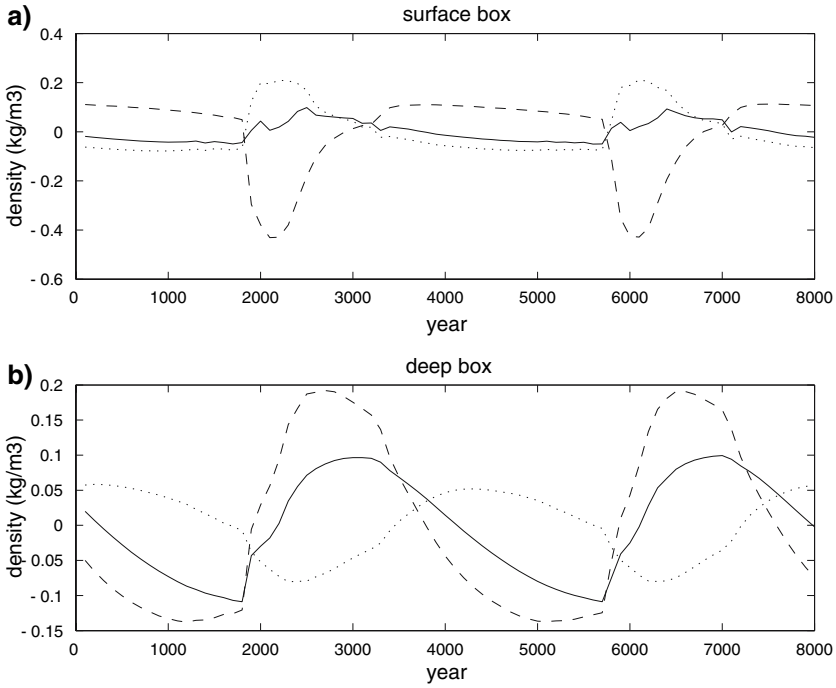

Fig. 5 Time series of potential temperature, salinity and density for two boxes of the Southern Ocean (*upper box*: surface to 130 m, *lower box* 1,000 m to bottom; both boxes have a meridional extent of 90°S to 61.2°S). All three parameters have been averaged spatially in each box and the temporal mean has been subtracted. Density (*solid line*), $\rho_0 \cdot \beta \cdot$ salinity (*dotted line*) and $-\rho_0 \cdot \alpha \cdot$ temperature (*dashed line*) are shown for the upper box (**a**) and lower box (**b**). The values for α, β and ρ_0 are 1.7×10^{-4}/K, 7.6×10^{-4} kg/g and 1,028 kg/m^3, respectively. Results from the equilibrium run with an atmospheric CO_2 concentration of 720 ppm

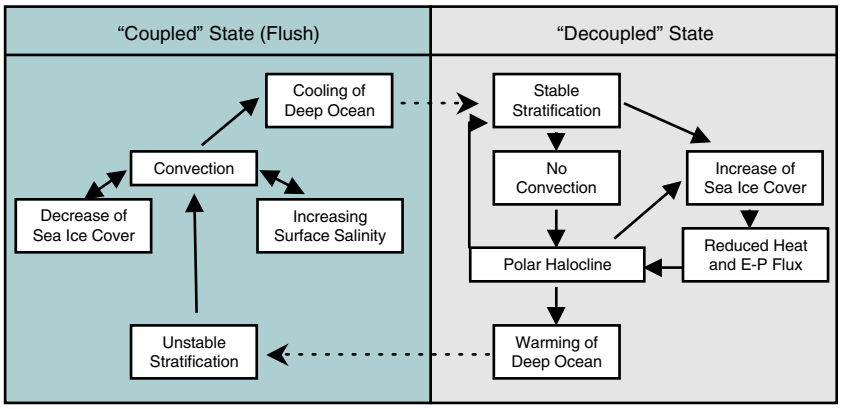

Fig. 6 Scheme describing the coupled and decoupled states in the model. After Fig. 8 in Haarsma et al. (2001)

Only the large-scale circulation is resolved in the model; the other three processes are parametrized. The effects of mesoscale eddies are modelled by the Gent and McWilliams (1990) mixing scheme through the so-called thickness layer diffusion, and also by isopycnal diffusion of temperature (both set to 800 m^2/s for the simulations described in this paper). The convection is parametrized by the scheme of Rahmstorf (1993). The small-scale vertical mixing due to turbulence is parametrized as diffusion, with vertical diffusivity following the Bryan and Lewis (1979) profile and ranging between 0.306×10^{-4} m^2/s and 1.304×10^{-4} m^2/s.

Between the flushes, the global mean potential temperature in the deep ocean increases. Convection normally removes heat from the deep ocean; if convection is suppressed or weakened, the sum of the reminding terms (LSC + MSE + SSM) is positive which leads to an accumulation of heat in the deep ocean. As in Haarsma et al. (2001), the main mechanism in our simulations is a downward heat transport through vertical diffusion from the tropical and midlatitude surface layers and a subsequent horizontal diffusion to the deep Antarctic Seas. A simple scale analysis of the diffusion processes leads to

$$\text{Horizontal diffusion}: \frac{\partial T}{\partial t} = K_{\mathrm{H}} \frac{\partial^2 T}{\partial y^2} \quad \text{or} \quad \tau = L^2/K_{\mathrm{H}} \tag{3}$$

$$\text{Vertical diffusion}: \frac{\partial T}{\partial t} = K_{\mathrm{V}} \frac{\partial^2 T}{\partial z^2} \quad \text{or} \quad \tau = H^2/K_{\mathrm{V}} \tag{4}$$

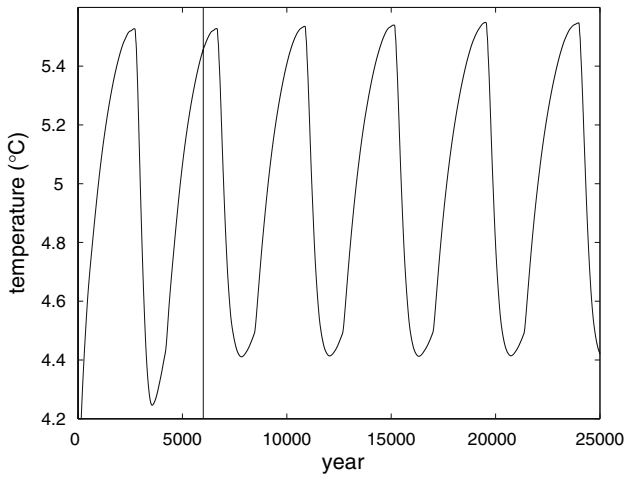

Fig. 7 Time series of the global mean ocean potential temperature in °C for a sensitivity study forced with an atmospheric CO_2 concentration of 720 ppm. After integration year 6000 (indicated by the *black vertical line*), the atmospheric winds are not allowed to react to the millennial-scale oscillations (seasonal winds are held constant)

where T is the potential temperature, t time, y latitude, z depth, and K_H and K_V are the horizontal and vertical diffusion coefficients, respectively. τ stands for the time scale and L and H for horizontal and vertical length scales, respectively. For $K_H = 800$ m^2/s, the time scale involved to transport heat horizontally across the Antarctic Circumpolar Current is of the order of magnitude of 100 years. Taking a mean value of 10^{-4} m^2/s for K_V and $H = 5{,}000$ m, τ is of the order of magnitude of 8,000 years for vertical diffusion which is consistent with the period of the oscillations described in this study.

With higher atmospheric CO_2 concentrations, the temperature of the surface layers increases, whereas the deep ocean potential temperatures after a flush are dictated by the surface temperature at deep convection sites and will always be near the freezing point. Therefore, the vertical temperature gradient increases with increasing atmospheric CO_2 concentration, which results in stronger and faster vertical diffusion of heat and a higher frequency of the oscillations. This phenomenon can be observed in our simulations: the periods of the oscillations decrease with increasing CO_2 concentrations (8,800, 6,200, 4,600, 4,400 and 3,900 years for the control runs under atmospheric CO_2 concentrations of 440, 480, 560, 640 and 720 ppm, respectively).

3.3 Wind fields and initial conditions

Although the oscillations described in the present study have been found in simpler models and are well understood, it is interesting to investigate how robust these oscillations are to changes in boundary conditions other than atmospheric CO_2 concentrations in the more comprehensive UVic ESCM. As the UVic ESCM atmospheric component is an energy moisture balance model, it cannot compute the dynamical behavior of the atmosphere. To take climate induced changes in the wind field into account, we added a ''wind feedback'' to present day wind data for all the control simulations described in this study. This method consists of the calculation of surface pressure anomalies via surface atmospheric temperature (SAT) anomalies. Wind and wind stress anomalies can

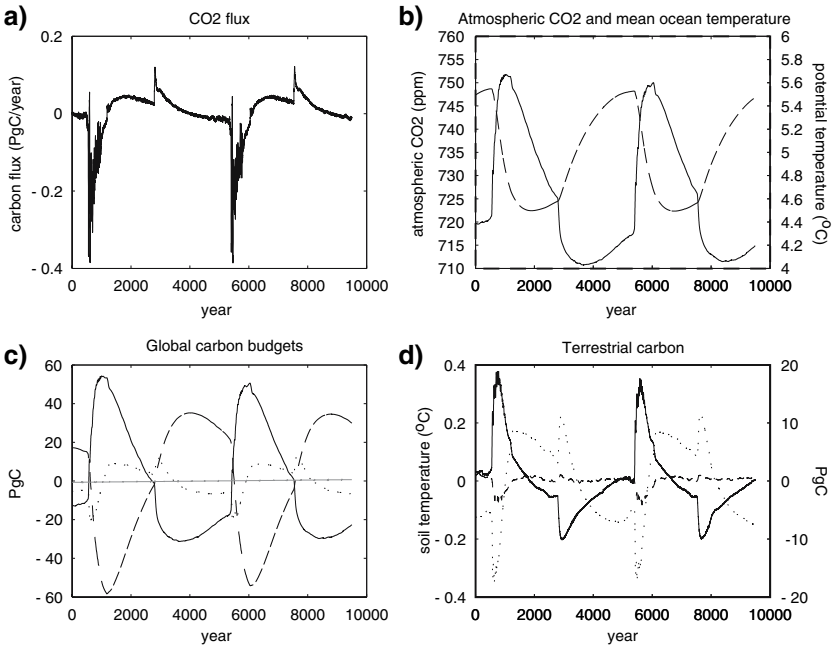

Fig. 8 Time series of **a** the globally integrated carbon flux into the ocean (in PgC/year), **b** atmospheric CO_2 concentrations (in ppm, *solid line*) and mean ocean potential temperature (in °C, *dashed line*), **c** global carbon budgets (minus mean value for each reservoir) in PgC, atmosphere (*solid line*), ocean (*dashed line*), terrestrial carbon (*dotted line*), global carbon (*solid gray line*), **d** terrestrial carbon (minus mean value for each reservoir) in PgC, soil carbon (*dotted line*), vegetation carbon (*dashed line*), and soil temperature (minus mean value, in °C, *solid line*)

then be calculated (see Weaver et al. 2001 for a detailed description); and are added to the NCEP data Kalnay et al. 1996. As this is probably one of the weakest points in the UVic ESCM, we conducted several sensitivity studies to analyze the role of the wind feedback in the described oscillations.

To test if the wind feedback triggers the oscillations, we ''froze'' the winds for a simulation under atmospheric CO_2 forcing of 720 ppm (see Fig. 7). In this sensitivity study (called 720_fixed hereafter), the wind feedback is held constant after integration year 6000, which is indicated by the vertical black line in Fig. 7. After year 6000, 720_fixed is forced by NCEP winds plus a fixed wind anomaly due to the different background climate compared to present day. Therefore the wind anomaly cannot react to the oceanic oscillations anymore. As can be seen in Fig. 7, the oscillations are not damped after integration year 6000, ruling out a mechanism which needs the atmospheric wind feedback in the UVic ESCM to trigger the convection events in the Southern Ocean.

The next question that arises is whether the fixed wind fields are triggering the oscillations. The fixed wind fields are the sum of climatological present day wind data (NCEP) and the wind anomaly calculated by the model and diagnosed from a control run. They depend on the background climate (surface temperature anomalies) and therefore on the atmospheric CO_2 concentration. Of special interest are the control runs with atmospheric CO_2 concentrations of 400 and 440 ppm because they are situated close to the threshold between non-oscillating and oscillating regimes. Table 1 summarizes the results of eight sensitivity experiments which were conducted with different initial conditions and wind forcings. Analyzing Table 1, several conclusions can be drawn:

- As already seen in Fig. 7, the interactive atmospheric feedback is not responsible for switching the system into an oscillatory regime. Runs B and D continue to oscillate although the wind feedback is not interactively coupled.
- More generally, the wind field used does not impact the result of whether or not the system gets into an oscillatory state. Runs A, B, C and D result in oscillations although they are forced with very different wind fields. Of special importance are runs C and D which were forced with PD climatological data and fixed 400 winds, respectively, and both continue to oscillate. On the other hand, runs F and G do not oscillate regardless of the inclusion of windstress feedback.
- There is no evidence that multiple equilibria can occur under the same boundary conditions. Run E is started from a non-oscillational control run (400) and starts oscillating, whereas run H is not oscillating, although it was started from an oscillating run.
- The CO_2 concentration and hence radiative forcing seems to be the only parameter in these sensitivity studies which defines if the system is oscillating or not.

We can therefore conclude that the oscillations are a robust feature in the UVic ESCM. The wind feedback parametrization does not seem to play an important role in the mechanism. The atmospheric CO_2 concentration, however, does. One possible mechanism that could explain the switch between oscillating and non-oscillating states involves the extent of sea ice in our simulations. For low concentrations of CO_2 the extent of sea ice over convective regions suppresses the ability of oscillations. With higher CO_2 concentrations, the sea ice retreats to higher latitudes and convective areas are close to the sea ice margins which makes oscillations possible.

Table 1 Sensitivity studies

Run	Initial conditions	CO2	Wind feedback	Oscillations
A	440	440	Free	Yes
B	440	440	440 fixed	Yes
C	440	440	None	Yes
D	440	440	400 fixed	Yes
E	400	440	Free	Yes
F	400	400	Free	No
G	400	400	None	No
H	440	400	Free	No

Initial conditions indicates which restarts were taken (for example: 440 = run started from the 440 control run with CO_2 concentrations = 440 ppm and a free wind feedback added to the NCEP data). CO_2 indicates the atmospheric CO_2 concentration with which the sensitivity run is forced. Wind feedback can be free (free wind feedback reacting each time step to climate change), fixed (wind feedback field extracted from a control run and kept constant during the integration) or none (no wind feedback, just NCEP climatological data). The last column indicates if the system is oscillating or not

3.4 Impact on the global carbon cycle

In order to investigate the impact that the millennial oscillations have on the global carbon cycle, the 720 control was rerun with the fully coupled carbon cycle. Figure 8a shows the time series of the globally integrated carbon flux at the air sea interface. During the flushes, the flux is negative. Deep water enriched in dissolved inorganic carbon (DIC) is brought to the surface where a net flux of oceanic inorganic carbon into the atmosphere takes place. It is the biological pump which is mainly responsible for the accumulation of DIC in the deep ocean and therefore for the sign of the atmosphere-ocean CO_2 flux during the flushes. This carbon accumulates in the atmosphere and

Table 2 Impact of the coupled carbon cycle on oscillations

	Coupled carbon cycle	720_fixed
ΔSAT	1.128°C	1.022°C
ΔSST	0.972°C	0.892°C
Δtbar	1.054°C	1.139°C
Δ sea ice area SH	6.6409×10^{12} m^2	6.7321×10^{12} m^2
Period	4,870 years	4,500 years
Δ kinetic energy	0.0037 J/m^3	0.0039 J/m^3

Δ stands for the difference between the maximum and minimum values in timeseries. SAT stands for global mean atmospheric surface temperature, SST for global mean sea surface temperature, tbar for global mean ocean potential temperature, sea ice area SH for the sea ice area in the Southern Hemisphere, period is the period of the oscillations and kinetic energy the global ocean kinetic energy density

results in an increase of the atmospheric concentration which reaches a maximum of 752 ppm (Fig. 8b). The increase in atmospheric carbon dioxide intensifies the atmospheric warming due to albedo and sea surface temperature (SST) changes. After the flush, the carbon flux becomes positive and atmospheric CO_2 is slowly taken up by the ocean again. The CO_2 flux shows a small positive spike around year 2800. This spike is due to the rapid last advance of sea ice in the Southern Hemisphere which causes a global cooling and decrease in precipitation. The consequences of this spike can also be seen in the global carbon budgets (Fig. 8c) and the terrestrial carbon time series (Fig. 8d). Once the Southern Hemisphere sea ice reaches its maximum extent, atmospheric CO_2 decreases more rapidly concurrent with a rapid increase in the mean ocean potential temperature (Fig. 8b). The amplitude of the oscillation in atmospheric CO_2 is 41 ppm (by amplitude we refer to the difference between maximum and minimum value).

Global carbon budgets are shown in Fig. 8c. The ocean and atmosphere are the two carbon reservoirs with the most important carbon exchange during the oscillations, the terrestrial carbon plays a minor role. Finally, Fig. 8d shows the variation in soil carbon, vegetation carbon and soil temperature. Changes in vegetation carbon are negligible on the global scale. Soil carbon varies opposite to the soil temperature because soil respiration increases with temperature (Cox 2001).

Whereas the oscillations impact the atmospheric CO_2 concentrations significantly, the inclusion of the carbon cycle affects the magnitude of the oscillations only slightly. To be able to compare integrations with and without carbon cycle, the coupled carbon experiment was run with the same wind fields used for 720_fixed. As can be seen in Table 2, the amplitude of global mean atmospheric surface temperatures is increased by 0.1°C when compared to 720_fixed. During the flushing events, atmospheric CO_2 increases enhancing the atmospheric warming due to SST and albedo changes. At the same time, the warming of global mean SSTs is amplified by 0.08°C. On the other hand, the amplitude of change in global mean potential ocean temperature decreases by 0.08°C when the carbon cycle is included. This small change is due to a small change in the efficiency of the flushes. Whereas the temperature profiles in the Southern Ocean before a flush are identical for the coupled and non-coupled run, the temperature in the deep ocean is slightly warmer after a flush (not shown) when the carbon cycle is coupled. Changes in Southern Hemispheric sea ice area reflect the same phenomenon (the amplitude decreases by 1.3%) and the period of oscillation is increased by 370 years. The change in global ocean kinetic energy density decreases by 0.0002 J/m^3 which corresponds to a change of 5%.

4 Discussion

4.1 Comparison with EcBilt

To the authors' knowledge, EcBilt is the only other coupled global model that has been able to capture similar oscillations. Although both climate models belong to the class of ''Models of Intermediate Complexity'' (Claussen et al. 2002), their physical and numerical structure is different. Whereas the UVic model consists of state-of-the-art ocean and sea ice models which are coupled to a simple atmosphere model (see Sect. 2), EcBilt was built on a different approach: The atmosphere model is a spectral T21 global three level quasi-geostrophic model with simple parametrizations for the diabatic processes (Opsteegh et al. 1998). An estimate of the ageostrophic terms in the vorticity and thermodynamic equations is included as a temporally and spatially varying forcing. For the study of Haarsma et al. (2001) the atmospheric model is coupled to a simple coarse resolution Geophysical Fluid Dynamics Laboratory (GFDL) type model and a thermodynamic sea ice model. The horizontal resolution is 5.6 times 5.6 degrees, the ocean model has 12 levels and a flat bottom.

Although the models are different, our results are very similar to the results published by Haarsma et al. (2001). This might indicate that the millennial-scale oscillations are a robust feature of the climate system (or at least of some climate models).

4.2 Paleoproxy evidence in the Southern Hemisphere

If the oscillations described in the present paper are realistic, the oscillating regime would exist in the real ocean for one or several specific combinations of boundary conditions, which might or might not have been reached in the

past. Unfortunately, the recent climate history of the planet depicts colder conditions and lower CO_2 concentrations than what we will encounter in the near future. The last interglacial with comparable and even slightly warmer conditions compared to today was 120,000 years ago and the resolution and abundance of paleoproxy data from this time are too poor to test our hypothesis. Furthermore, the atmospheric CO_2 concentration did not exceed 310 ppm for at least the last 800,000 years. It is nevertheless interesting to investigate if paleoproxy data from the recent past indicate the existence of millennial oscillations with similar characteristics, as an oscillatory regime sharing the same physical mechanism might be reached for several different boundary conditions.

Numerous publications have discussed millennial timescale oscillations and their role in the global climate. One of the main findings is that millennial-scale oscillations, although existent throughout the records, are most pronounced during episodes with intermediate ice volume. Furthermore, the paleoproxy records suggest the existence of two spatially distinct signals, the Dansgaard-Oeschger events in the Northern Hemisphere and the A-events in the Southern Hemisphere [for a thorough overview, the reader is referred to Clark et al. (2007)]. We will focus in this Section on the millennial-scale warmings in Antarctica (the so-called A-events).

The imprint of millennial-scale oscillations in Antarctica and the Southern Ocean can be found in ice rafted debris (IRD), planktic $\delta^{18}O$ values (Kanfoush et al. 2000, 2002) and sea surface temperature (SST) reconstructions in the southeast Pacific (Kaiser et al., 2005) amongst others. Blunier and Brook (2001) emphasized the spatial scale of these oscillations and stated: ''The similarity of inner Antarctic ice core records and many Southern Ocean SST records suggest that the timing of millennial-scale climate variability that we infer for Byrd characterized a large area of the Antarctic continent and Southern Ocean and has importance for understanding millennial-scale climate variability.''

There is also evidence that oscillations of the atmospheric CO_2 concentrations were synchronous with warming events in Antarctica (Indermühle et al. 2000), with atmospheric CO_2 concentrations peaking during the warm A-events. A study conducted by Martin et al. (2005) used climate models to estimate the slope of co-variation between atmospheric CO_2 concentration and deep ocean temperature for (a) the temperature-dependent solubility of CO_2 in seawater and (b) the atmospheric CO_2-dependent radiative forcing for temperature. Paleoproxy data from the deglaciation and from marine isotope stage 3 (MIS 3) were then compared to the constructed slopes. The authors concluded that different mechanisms were driving the atmospheric CO_2 variability. Changes over the deglaciation were consistent with a scenario where atmospheric CO_2 changes, combined with ice albedo changes, were driving the temperature change. On the other hand, millennial-scale variability during MIS 3 could be explained by temperature-dependent solubility of the deep ocean driving the atmospheric CO_2. Variability in the production of Antarctic Bottom Water, such as the flushes described in the present study, might have been the cause for changes in deep ocean temperatures, CO_2 solubility and therefore CO_2 concentrations in the atmosphere. Along the same lines, a planktic $\delta^{13}C$ record from the South Atlantic (Charles et al. 1996) shows a shift of 0.6 to 0.8‰ during A-events, which cannot be explained by sea surface temperature changes only (Broecker and Maier-Reimer 1992). One possible scenario, which would explain the shift in $\delta^{13}C$, is the outgassing of CO_2 from nutrient rich deep-water (Clark et al. 2007). Additional evidence for an increase in nutrient supply from the Southern Ocean due to a weakening of stratification comes from $\delta^{15}N$ records (Robinson et al. 2007), alkenone concentrations and organic flux to the sea floor (Sachs and Anderson 2005; Clark et al. 2007).

We can therefore conclude that there is increasing evidence that the Southern Hemisphere has played an important role in past millennial timescale climate oscillations (Kanfoush et al. 2000, 2002; Kaiser et al. 2005; Blunier and Brook 2001). Furthermore, variability in atmospheric CO_2 on millennial timescales seems to be linked to warm events in the Southern Hemisphere (A-events, Indermühle et al. 2000), the variability in deep ocean temperatures (Martin et al. 2005) and changes in stratification and nutrient supply (Charles et al. 1996; Sachs and Anderson 2005; Robinson et al. 2007; Clark et al. 2007).

4.3 Possible impact on climate change scenarios

The UVic ESCM steps over a critical threshold for an atmospheric CO_2 concentration between 400 and 440 ppm. The present day concentration equals 383 ppm (Mauna Loa record, 2007), the mean annual increase 2.28 ppm per year (averaged over the last 5 years). The concentration of 400 ppm will be reached before 2020 and 440 ppm some time between the years 2020 and 2040 (Houghton et al. 2001).

Although the threshold set by the UVic ESCM could be reached during our life time, the reader should keep in mind that the present study is a sensitivity study carried out with a climate model that incorporates an important number but not all of the climate feedbacks that can play a role in global warming scenarios. The result should therefore be taken qualitatively and not quantitatively. The UVic ESCM starts oscillating for high CO_2 concentrations, which is in

agreement with the EcBilt study (the EcBilt simulation had a positive temperature anomaly in the Southern Ocean; Reindert Haarsma, personal communication).

The most important question arising from the described simulations is: How realistic are these oscillations? Are they an artifact of coarse resolution ocean models, which may overestimate the diffusion processes? If the mechanism described here is realistic, these type of oscillations will exist in the real world and in other climate models under certain boundary conditions. The present study made a first step, exploring the parameter domain with regard to the atmospheric CO_2 concentration.

As already mentioned in the Introduction, coupled atmosphere-ocean general circulation models (AOGCMs) indicate the existence of multiple steady states; as of today their computational expense is too high however to investigate millennial-scale oscillations. We hope that with increasing computing power more modelling groups will explore the existence and characteristics of this type of non-linear oscillations and their relation to global warming scenarios. One important result of the IPCC TAR report (Houghton et al. 2001) relates global warming to an increase in stratification in the ocean and a weakening of the thermohaline circulation (and therefore deep water formation). Both trends reinforce the decoupling of the surface and deep ocean and therefore make an oscillatory regime as described in the present study more likely.

5 Conclusions

We present several equilibrium runs under varying atmospheric CO_2 concentrations using version 2.8 of the University of Victoria Earth System Climate Model (UVic ESCM). The model shows two very different responses: for CO_2 concentrations below 440 ppm, the system gets into an equilibrium state. For high CO_2 concentrations, the system starts oscillating between a state with vigorous deep water formation in the Southern Ocean and a state with no deep water formation in the Southern Ocean. Deep water formation in the North Atlantic is only slightly affected by these oscillations. The flushing episodes result in a rapid increase in atmospheric temperatures, degassing of CO_2 and therefore an increase of atmospheric CO_2 concentrations and a reduction of sea ice cover in the Southern Ocean. They also cool the deep ocean worldwide. After the flush, the deep ocean warms slowly again and CO_2 is taken up by the ocean until the stratification becomes unstable again at high latitudes thousands of years later. Although the mechanism of thermally driven millennial-scale oscillations has been known for decades, only two global coupled models with realistic boundary conditions have found evidence of such a behavior so far (Haarsma et al. 2001, and the present study). It has not been found in coupled atmosphere ocean general circulation models (AOGCMs), probably because simulations with AOGCMs are too expensive to be run long enough to reveal millennial timescale oscillations. The existence of a threshold in CO_2 concentration which places the UVic ESCM in either an oscillating or non-oscillating state is intriguing. If the UVic ESCM captures a mechanism that is present and important in the real climate system, the consequences would comprise a rapid increase in CO_2 of several tens of ppm, an increase in global surface temperature in the order of 1–2°C, local temperature changes of the order of 6°C and a profound change in ocean stratification, deep water temperature and sea ice cover.

Acknowledgments We would like to thank Ed Wiebe for his technical assistance. We are also grateful to Reindert Haarsma and two anonymous reviewers for their helpful and constructive comments. This research was supported by grants from the Natural Science and Engineering Research Council of Canada (NSERC) and the Canadian Foundation for Climate and Atmospheric Sciences (CFCAS) sponsored Polar Climate Stability Network.

References

Blunier T, Brook EJ (2001) Timing of millenial-scale climate change in Antarctica and Greenland during the last glacial period. Science 291:109–112

Bond G, Showers W, Cheseby M, Lotti R, Almasi P, deMenocal P, Priore P, Cullen H, Hajdas I, Bonani G (1997) A pervasive millennial-scale cycle in North Atlantic Holocene and glacial climates. Science 278:1257–1266

Bond G, Kromer B, Beer J, Muscheler R, Evans M, Showers W, Hoffmann S, Lotti-Bond R, Hajdas I, Bonani G (2001) Persistent solar influence on North Atlantic surface circulation during the Holocene. Science 294:2130–2136

Braun H, Christl M, Rahmstorf S, Ganopolski A, Mangini A, Kubatzki C, Roth K, Kromer B (2005) Solar forcing of abrupt glacial climate change in a coupled climate system model. Nature 438:208–211

Broecker WS, Maier-Reimer E (1992) The influence of air and sea exchange on the carbon isotope distribution in the sea. Global Biogeochem Cycles 6:315–320

Bryan F (1986) High-latitude salinity effects and interhemispheric thermohaline circulations. Nature 323:301–304

Bryan K, Lewis L (1979) A water mass model of the world ocean. J Geophys Res 84:311–337

Charles CD, Lynch-Stieglitz J, Ninnemann US, Fairbanks RG (1996) Climate connections between the hemispheres revealed by deep sea sediment core/ice core correlations. Earth Planet Sci Lett 142:19–27

Clark PU, Pisias NG, Stocker TF, Weaver AJ (2002) The role of the thermohaline circulation in abrupt climate change. Nature 415:863–869

Clark PU, Hostetler SW, Pisias NG, Schmittner A, Meissner KJ (2007) Past and future changes of the ocean meridional overturning circulation: mechanisms and impacts, Chap. Mechanisms for a ~7-kyr climate and sea-level oscillation during marine isotope stage 3. AGU Monograph, submitted

Claussen M, Mysak LA, Weaver AJ, Crucifix M, Fichefet T, Loutre MF, Weber SL, Alcamo J, Alexeev VA, Berger A, Calov R, Ganopolski A, Goosse H, Lohmann G, Lunkeit F, Mokhov BB, Petoukhov V, Stone P, Wang Z (2002) Earth system models of intermediate complexity: closing the gap in the spectrum of climate models. Climate Dyn 18:579–586

Collatz GJ, Ball JT, Grivet C, Berry JA (1991) Physiological and environmental regulation of stomatal conductance, photosynthesis and transpiration: a model that includes a laminar boundary layer. Agric For Meteorol 54:107–136

Collatz GJ, Ribas-Carbo M, Berry JA (1992) A coupled photosynthesis-stomatal conductance model for leaves of C_4 plants. Aust J Plant Physiol 19:519–538

Cox PM (2001) Description of the 'TRIFFID' dynamic global vegetation model. Hadley Centre technical note 24:1–16

Cox PM, Huntingford C, Harding RJ (1999) A canopy conductance and photosynthesis model for use in a GCM land surface scheme. J Hydrol 212-213:79–94

Cox PM, Betts RA, Jones CD, Spall SA, Totterdell IJ (2000) Acceleration of global warming due to carbon-cycle feedbacks in a coupled climate model. Nature 408:184–187

Ewen TL, Weaver AJ, Eby M (2004) Sensitivity of the inorganic carbon cycle to future climate warming in the UVic coupled model. Atmos Ocean 42:23–42

Gent PR, McWilliams JC (1990) Isopycnal mixing in ocean general circulation models. J Phys Oceanogr 20:150–155

Haarsma RJ, Opsteegh JD, Selten FM, Wang X (2001) Rapid transitions and ultra-low frequency behaviour in a 40 kyr integration with a coupled climate model of intermediate complexity. Climate Dyn 17:559–570

Hibler WD (1979) A dynamic thermodynamic sea ice model. J Phys Oceanogr 9:815–846

Hinnov LA, Schulz M, Yiou P (2002) Interhemispheric space-time attributes of the Dansgaard-Oeschger oscillations between 100 and 0 ka. Quat Sci Rev 21:1213–1228

Houghton JT, Ding Y, Griggs DJ, Noguer M, van der Linden PJ, Dai X, Maskell K, Johnson CA (eds) (2001) Climate change 2001: the scientific basis. IPCC Third Assessment Report, Cambridge University Press

Hunke EC, Dukowitz JK (1997) An elastic-viscous-plastic model for sea ice dynamics. J Phys Oceanogr 27(9):1849–1867

Indermühle A, Monnin E, Stauffer B, Stocker TF (2000) Atmospheric CO_2 concentration from 60 to 20 kyr BP from the Taylor Dome ice core, Antarctica. Geophys Res Lett 27(5):735–738

Kaiser J, Lamy F, Hebbeln D (2005) A 70-kyr sea surface temperature record off southern Chile (Ocean Drilling Program Site 1233). Paleoceanography 20(4):PA4009

Kalnay E, Kanamitsu M, Kistler R, Collins W, Deaven D, Gandin L, Iredell M, Saha S, White G, Woollen J, Zhu Y, Chelliah M, Ebisuzaki W, Higgins W, Janowiak J, Mo KC, Ropelewski C, Wang J, Leetma A, Reynolds R, Jenne R, Joseph D (1996) The NCEP/NCAR 40-year reanalysis project. Bull Am Met Soc 77(3): 437–471

Kanfoush SL, Hodell DA, Charles CD, Guilderson TP, Mortyn PG, Ninnemann US (2000) Millenial-scale instability of the Antarctic ice sheet during the last glaciation. Science 288:1815–1818

Kanfoush SL, Hodell DA, Charles CD, Janecek TR, Rack FR (2002) Comparison of ice-rafted debris and physical properties in ODP Site 1094 (South Atlantic) with the Vostock ice core over the last four climatic cycles. Palaeogeogr Palaeoclimatol Palaeoecol 182(3-4):329–349

Lenderink G, Haarsma RJ (1994) Variability and multiple equilibria of the thermohaline circulation associated with deep water formation. J Phys Oceanogr 24:1480–1493

Leuschner DC, Sirocko F (2000) The low-latitude monsoon climate during Dansgaard-Oeschger cycles and Heinrich Events. Quat Sci Rev 19:243–254

Marotzke J (1989) Oceanic circulation models: combining data and dynamics, Chap. Instabilities and multiple steady states of the thermohaline circulation. NATO ASI series, Kluwer, pp 501–511

Marotzke J (1990) Instabilities and multiple equilibria of the thermohaline circulation. Ph.D. thesis, Ber. Inst. Meeresk. Kiel

Marotzke J, Welander P, Willebrand J (1988) Instability and multiple steady states in a meridional-plane model of the thermohaline circulation. Tellus 40A:162–172

Martin P, Archer D, Lea DW (2005) Role of deep sea temperature in the carbon cycle during the last glacial. Paleoceanography 20(PA2015):1–10

Matthews HD, Weaver AJ, Meissner KJ (2005) Terrestrial carbon cycle dynamics under recent and future climate change. J Climate 18:1609–1628

Meissner KJ, Weaver AJ, Matthews HD, Cox PM (2003) The role of land surface dynamics in glacial inception: a study with the UVic Earth System Model. Climate Dyn 21:515–537

Mikolajewicz U, Maier-Reimer E (1994) Internal secular variability in an ocean circulation model. Climate Dyn 4:145–156

Muscheler R, Beer J (2006) Solar forced Dansgaard/Oeschger events? Geophys Res Lett 33(L20706):1–4

Opsteegh JD, Haarsma RJ, Selten FM, Kattenberg A (1998) ECBILT: a dynamic alternative to mixed boundary conditions in ocean models. Tellus 50A:348–367

Pacanowski RC (1995) MOM 2 documentation, user's guide and reference manual. Tech. Rep. 3, GFDL Ocean Group, Geophysical Fluid Dynamics Laboratory, Princeton

Partridge TC (2002) Were Heinrich events forced from the Southern Hemisphere? South Afr J Sci 98(1/2)

Power SB, Kleeman R (1994) Surface flux parameterisation and the response of OGCMs to high latitude freshening. Tellus 46A:86–95

Rahmstorf S (1993) A fast and complete convection scheme for ocean models. Ocean Modell 101:9–11

Rahmstorf S (1995) Bifurcations of the Atlantic thermohaline circulation in response to changes in the hydrological cycle. Nature 378:145–149

Ramaswamy V, Boucher O, Haigh J, Hauglustaine D, Haywood J, Myhre G, Nakajima T, Shi GY, Solomon S, Betts R, Charlson R, Chuang C, Daniel JS, Del Genio A, van Dorland R, Feichter J, Fuglestvedt J, Forster PMdF, Ghan SJ, Jones A, Kiehl JT, Koch D, Land C, Lean J, Lohmann U, Minschwaner K, Penner JE, Roberts DL, Rodhe H, Roelofs GJ, Rotstayn LD, Schneider TL, Schumann U, Schwartz SE, Schwarzkopf MD, Shine KP, Smith S, Stevenson DS, Stordal F, Tegen I, Zhang Y (2001) Climate Change 2001: The Scientific Basis. Contribution of Working Group I to the Third Assessment Report of the Intergovernmental Panel on Climate Change, chap. Radiative forcing of climate change. Cambridge University Press, UK, pp. 350–416

Robinson RS, Mix A, Martinez P (2007) Southern Ocean control on the extent of denitrification in the southeast Pacific over the last 70 ka. Quat Sci Rev 26:201–212

Sachs JP, Anderson RF (2005) Increased productivity in the subantarctic ocean during Heinrich events. Nature 434:1118–1121

Sakai K, Peltier WR (1997) Dansgaard-Oeschger oscillations in a coupled atmosphere-ocean climate model. J Climate 10:949–970

Schartau M, Oschlies A (2003) Simultaneous data-based optimization of a 1D-ecosystem model at three locations in the North Atlantic: Part I - Method and parameter estimates. J Mar Res 61:765–793

Schmittner A (2005) Decline of the marine ecosystem caused by a reduction in the Atlantic overturning circulation. Nature 434:628–633

Schmittner A, Saenko OA, Weaver AJ (2003) Coupling of the hemispheres in observations and simulations of glacial climate change. Quat Sci Rev 22:659–671

Schmittner A, Oschlies A, Giraud X, Eby M, Simmons HL (2005) A global model of the marine ecosystem for long-term simulations: Sensitivity to ocean mixing, buoyancy forcing, particle sinking, and dissolved organic matter cycling. Global Biogeochem Cycles 19:GB3004:1–17

Schmittner A, Oschlies A, Matthews HD, Galbraith ED (2007) Future changes in climate, ocean circulation, ecosystems and biogeochemical cycling simulated for a business-as-usual CO_2 emission scenario until year 4000 AD. Global Biogeochem Cycles (submitted)

Semtner AJJ (1976) A model for the thermodynamic growth of sea ice in numerical investigations of climate. J Phys Oceanogr 6(3):379–389

Shackleton N (2001) Paleoclimate: climate change across the Hemispheres. Science 291(5501):58–59

Tziperman E, Toggweiler JR, Feliks Y, Bryan K (1994) Instability of the thermohaline circulation with respect to mixed boundary conditions: Is it really a problem for realistic models? J Phys Oceanogr, pp 217–232

Weaver AJ (1999) Millennial timescale variability in ocean/climate models. In: Webb R, Clark P, Keigwin L (eds) Mechanisms of global climate change at millennial time scales no 112 in geophysical monograph series. American Geophysical Union, Washington, DC

Weaver A, Hughes TMC (1992) Stability and variability of the thermohaline circulation and its link to climate. Trends in Physical Oceanography Research Trends Series Council of Scientific Research Integration Trivandrum India 1:15–70

Weaver AJ, Hughes TMC (1994) Rapid interglacial climate fluctuations driven by North Atlantic ocean circulation. Nature 367:447–450

Weaver AJ, Sarachik ES (1991) Evidence for decadal variability in an ocean general circulation model: an advective mechanism. Atmos Ocean 29:197–231

Weaver AJ, Eby M, Wiebe EC, Bitz CM, Duffy PB, Ewen TL, Fanning AF, Holland MM, MacFadyen A, Matthews HD, Meissner KJ, Saenko O, Schmittner A, Wang H, Yoshimori M (2001) The UVic Earth System Climate Model: model description, climatology, and applications to past, present and future climates. Atmos Ocean 4:361–428

Welander P (1982) A simple heat-salt oscillator. Dyn Atmos Ocean 6:233–242

Winton M (1993) Ice in the climate system, Chap. Deep decoupling oscillations of the oceanic thermohaline circulation. Springer, Heidelberg, pp 417–432

Winton M (1995) Energetics of deep-decoupling oscillations. J Phys Oceanogr 25:420–427

Winton M (1997) The effect of cold climate upon North Atlantic Deep Water formation in a simple ocean-atmosphere model. J Climate 10:37–51

Winton M, Sarachik ES (1993) Thermohaline oscillations induced by strong steady salinity forcing of ocean general circulation models. J Phys Oceanogr 23:1389–1410

Wright DG, Stocker TF (1991) A zonally averaged ocean model for the thermohaline circulation. Part I: Model development and flow dynamics. J Phys Oceanogr 21:1713–1724

Zhang S, Greatbach RJ, Lin CA (1993) A reexamination of the polar halocline catastrophe and implications for coupled ocean-atmosphere modeling. J Phys Oceanogr 23:287–299